11/15/95

SANDIA REPORT

SAND95–2405 • UC–706
Unlimited Release
Printed November 1995

An Overview of Fast Multipole Methods

James H. Strickland, Roy S. Baty

Prepared by
Sandia National Laboratories
Albuquerque, New Mexico 87185 and Livermore, California 94550
for the United States Department of Energy
under Contract DE-AC04-94AL85000

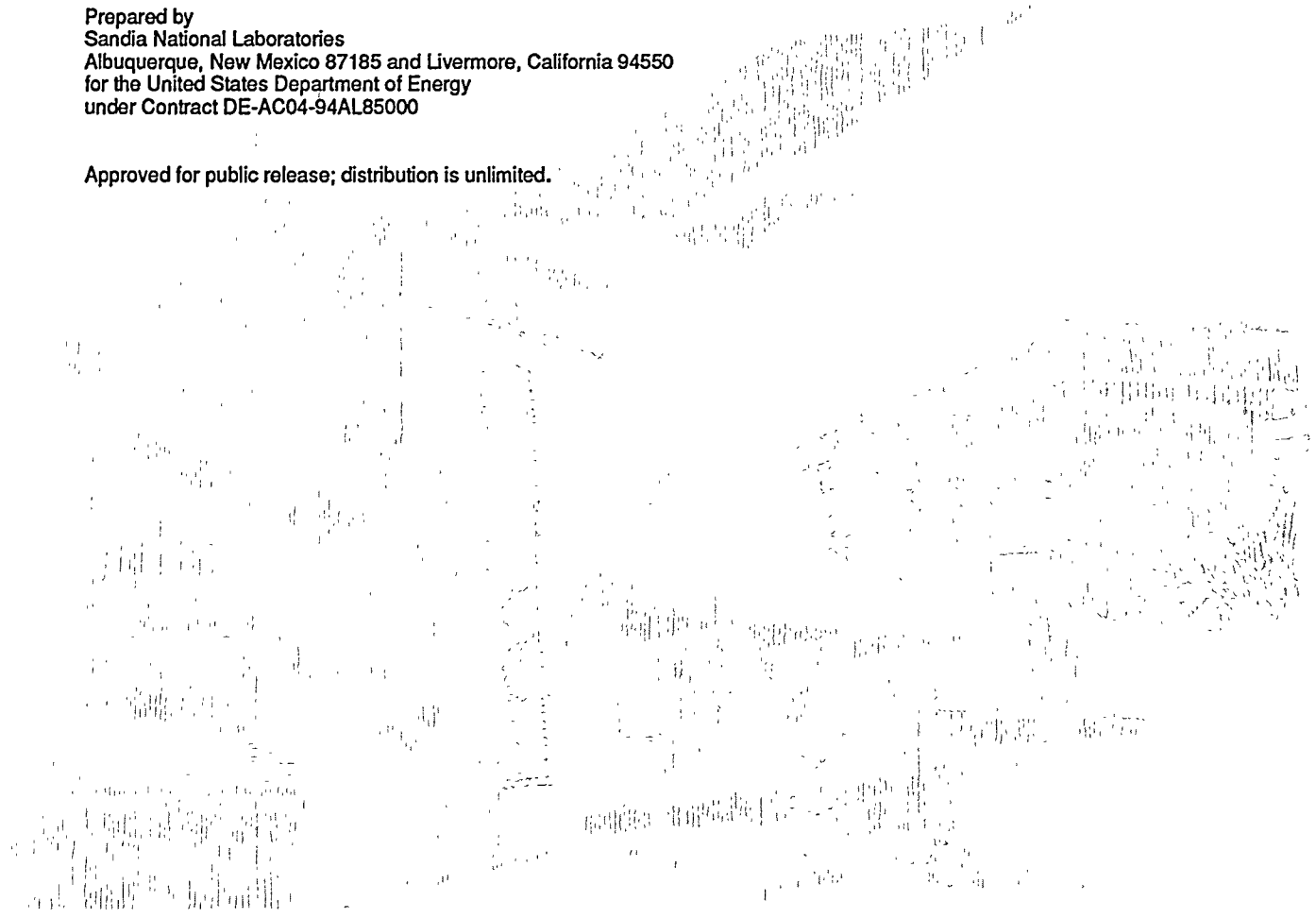

Issued by Sandia National Laboratories, operated for the United States Department of Energy by Sandia Corporation.

Available to DOE and DOE contractors from
Office of Scientific and Technical Information
PO Box 62
Oak Ridge, TN 37831

Prices available from (615) 576-8401, FTS 626-8401

Available to the public from
National Technical Information Service
US Department of Commerce
5285 Port Royal Rd
Springfield, VA 22161

NTIS price codes
Printed copy: A03
Microfiche copy: A01

SAND95-2405
Unlimited Release
Printed November 1995

Distribution
Category UC-706

An Overview of Fast Multipole Methods

James H. Strickland
Roy S. Baty

Engineering Sciences Center
Sandia National Laboratories
Albuquerque, New Mexico 87185

Abstract

A number of physics problems may be cast in terms of Hilbert-Schmidt integral equations. In many cases, the integrals tend to be zero over a large portion of the domain of interest. All of the information is contained in compact regions of the domain which renders their use very attractive from the standpoint of efficient numerical computation. Discrete representation of these integrals leads to a system of N elements which have pair-wise interactions with one another. A direct solution technique requires computational effort which is $O(N^2)$. Fast multipole methods (FMM) have been widely used in recent years to obtain solutions to these problems requiring a computational effort of only $O(N\ln N)$ or $O(N)$. In this paper we present an overview of several variations of the fast multipole method along with examples of its use in solving a variety of physical problems.

Presented at the Quadrature and Fast Algorithms workshop of the AMS-SIAM Summer Seminar, Park City Utah, Aug 7-9, 1995.

(this page intentionally left blank)

Nomenclature

f	Arbitrary function
k	Positive constant
m	Summation index
n	Summation index
p	Summation bound
q	Summation index
r	Radial coordinate
x	Coordinate
$\underset{\sim}{x}$	Vector coordinate
u	Arbitrary function
$\underset{\sim}{u}$	Velocity vector
A_j	Functions from separation of variables
$\underset{\sim}{A}^m{}_n$	Coefficients for spherical harmonics
B_j	Functions from separation of variables
C_j	Pre-computed coefficients
C'_j	Shifted coefficients
D	Divergence of the velocity
H_n	Hermite polynomials
J_1	Bessel function
K	Integral kernel function (Green's function)
L	Arbitrary linear operator
N	Summation bound
W	Function
$\underset{\sim}{W}$	Vector function
$Y_n{}^m$	Spherical harmonics

Nomenclature (continued)

α	Positive constant
ε	Truncation error
ψ	Stream-function
$\underline{\psi}$	Vector potential
ϕ	Angular coordinate
θ	Angular coordinate
$\underline{\omega}$	Vorticity vector

Table of Contents

(this page intentionally left blank)

1 INTRODUCTION

Many problems in science and engineering can be cast in terms of integral equations of the form:

$$\psi(\underset{\sim}{x}) = \int W(\underset{\sim}{x}') K(\underset{\sim}{x}, \underset{\sim}{x}')\, dx' \tag{1}$$

for which a discrete form may be written in terms of the summation:

$$\psi(\underset{\sim}{x}) = \sum_{i=1}^{N} W(\underset{\sim}{x}'_i) K(\underset{\sim}{x}, \underset{\sim}{x}'_i)\ . \tag{2}$$

For example, Roach [1] shows that the solutions for a large class of linear differential equations given by $Lu = f$ where L is a linear differential operator may be cast in this form when L^{-1} exists. In this case, the kernel $K(\underset{\sim}{x}, \underset{\sim}{x}')$ is a Green's function for the operator L and $W(\underset{\sim}{x}') = f$. Examples of classical physics problems which may be cast in terms of Equation 2 as noted by Greengard [2] include N body gravitational problems, electrostatic fields, magneto-statics, heat conduction, and acoustic fields. Several example kernels $K(\underset{\sim}{x}, \underset{\sim}{x}')$ are given in Table 1.

No.	$K(\underset{\sim}{x}, \underset{\sim}{x}'_i)$	Physical interpretation of $\psi(\underset{\sim}{x})$
1	$\ln\left(\lvert\underset{\sim}{x} - \underset{\sim}{x}'_i\rvert\right)$	two-dimensional electrostatic potential and two-dimensional stream-function for vortex flows
2	$\dfrac{\underset{\sim}{x} - \underset{\sim}{x}'_i}{\lvert\underset{\sim}{x} - \underset{\sim}{x}'_i\rvert^3}$	three-dimensional gravitational force, force due to charged particles, velocity associated with a field of vorticity, Biot-Savart law
3	$e^{-\alpha\lvert\underset{\sim}{x} - \underset{\sim}{x}'_i\rvert^2}$	temperature due to heat conduction, diffusion
4	$\dfrac{e^{i\alpha\lvert\underset{\sim}{x} - \underset{\sim}{x}'_i\rvert}}{\lvert\underset{\sim}{x} - \underset{\sim}{x}'_i\rvert}$	three-dimensional acoustic pressure
5	$r'_i r \int_0^\infty e^{-k\lvert x - x'_i\rvert} J_1(kr'_i) J_1(kr)\, dk$	axisymmetric stream-function for vortex rings

Table 1: Example Kernel Functions

The primary interest of the authors in this subject area involves the use of fast algorithms to facilitate computations associated with gridless vortex methods in fluid mechanics. In these methods, it is necessary to obtain the velocity vector $\underset{\sim}{u}(\underset{\sim}{x})$ in terms of the vorticity vector $\underset{\sim}{\omega}(\underset{\sim}{x}')$ and the divergence of the velocity field $D(\underset{\sim}{x}')$. Use of the Helmholtz decomposition for a vector field [3] allows us to accomplish this:

$$\underset{\sim}{u}(\underset{\sim}{x}) = \nabla \times \int_{R_\infty} \underset{\sim}{\omega}(\underset{\sim}{x}') K(\underset{\sim}{x}, \underset{\sim}{x}') \, dR(\underset{\sim}{x}') - \nabla \int_{R_\infty} D(\underset{\sim}{x}') K(\underset{\sim}{x}, \underset{\sim}{x}') \, dR(\underset{\sim}{x}') . \tag{3}$$

From Equation 2 one notes that in order to carry out a direct summation for N target points located at various values of $\underset{\sim}{x}$, a computational effort of order N^2 is required. This becomes very expensive for systems in which N exceeds 10^3 to 10^4. In many cases, one would like to make calculations with N on the order of 10^6 to 10^9 which is not practical using direct summation.

However, in the event that Equation 1 is a Hilbert-Schmidt integral equation [4], the kernel $K(\underset{\sim}{x}, \underset{\sim}{x}'_i)$ may be approximated by a degenerate kernel of the form:

$$K(\underset{\sim}{x}, \underset{\sim}{x}'_i) = \sum_{j=1}^{p} A_j(\underset{\sim}{x}'_i) B_j(\underset{\sim}{x}) \tag{4}$$

which produces a discrete problem requiring a computational effort of order Np. This can be achieved by first substituting Equation 4 into Equation 2 and rearranging the order of summation to yield:

$$\psi(\underset{\sim}{x}) = \sum_{j=1}^{p} B_j(\underset{\sim}{x}) \sum_{i=1}^{N} W(\underset{\sim}{x}'_i) A_j(\underset{\sim}{x}'_i) . \tag{5}$$

We now define the coefficients $C_j(\underset{\sim}{x}'_i)$ by:

$$C_j(\underset{\sim}{x}'_i) \equiv \sum_{i=1}^{N} W(\underset{\sim}{x}'_i) A_j(\underset{\sim}{x}'_i) \tag{6}$$

so that:

$$\psi(\underset{\sim}{x}) = \sum_{j=1}^{p} B_j(\underset{\sim}{x}) C_j(\underset{\sim}{x}'_i) . \tag{7}$$

The coefficients $C_j(\underset{\sim}{x}'_i)$ are computed using Equation 6 prior to carrying out the summation indicated in Equation 7. Computation of $C_j(\underset{\sim}{x}'_i)$ requires $O(Np)$ work. Since the summation in Equation 7 for all N target points at $\underset{\sim}{x}$ also requires $O(Np)$ work we see that this method requires $O(Np)$ work as opposed to $O(N^2)$ work associated with the direct solution of Equation 2. Obviously p must be significantly less than N for this scheme to provide a significant advantage.

It should be emphasized that the fast algorithm (Equation 7) is based on the fact that only information at $\underset{\sim}{x}'$ is required to obtain the precomputed coefficients $C_j(\underset{\sim}{x}'_i)$. This is, in turn, based on the ability to obtain the "separation of variables" indicated by the right hand side of Equation 4. In many problems of interest, Equation 4 is obtained from a truncated series which has a limited range of validity for a specified level of accuracy. For example the kernel $K(\underset{\sim}{x}, \underset{\sim}{x}'_i)$ might be represented by a truncated Laurent series or some other far-field representation which requires that the target point $\underset{\sim}{x}$ be far away or "well separated" from the source located at $\underset{\sim}{x}'_i$. On the other hand, the truncated series might be a Taylor series or some other near-field expansion written about some point near to a set of target points but well separated from the source points. The term "multipole expansion" has been used by Greengard and Rokhlin [6] to indicate the far-field series expansion and the term "local expansion" to indicate the near-field series expansion. This terminology will be adopted for the purposes of this paper.

As indicated, for most problems of interest, Equation 4 will be represented by multipole or local series expansions which are valid to some specified level of accuracy according to the relative separation of target and source points. Since the target and source points may, in general, be located anywhere within the domain of interest, somewhat elaborate schemes must be employed to insure that the series expansions are properly used. There are two major classes of methods which have been developed to accomplish this. The so called "hierarchical" or "tree code" schemes typified by the Barnes-Hut algorithm [5] use only multipole expansions while the Greengard Rokhlin algorithm [6] makes use of both multipole and local expansions.

2 SERIES EXPANSIONS

In this section, we will present examples of Equation 4 for several different physical problems which can be represented by multipole or local series expansions.

2.1 Multipole

In Figure 1 the geometry associated with the multipole expansion is represented. The source points are located inside the domain D_1 at points $\underset{\sim}{x}'_i$. The multipole expansion is constructed about the point $\underset{\sim}{x}_{sc}$ in D_1 and the target point is located outside of domain D_1 at the point $\underset{\sim}{x}$. It is assumed that a series expansion which is accurate to some precision can be obtained at the point $\underset{\sim}{x}$.

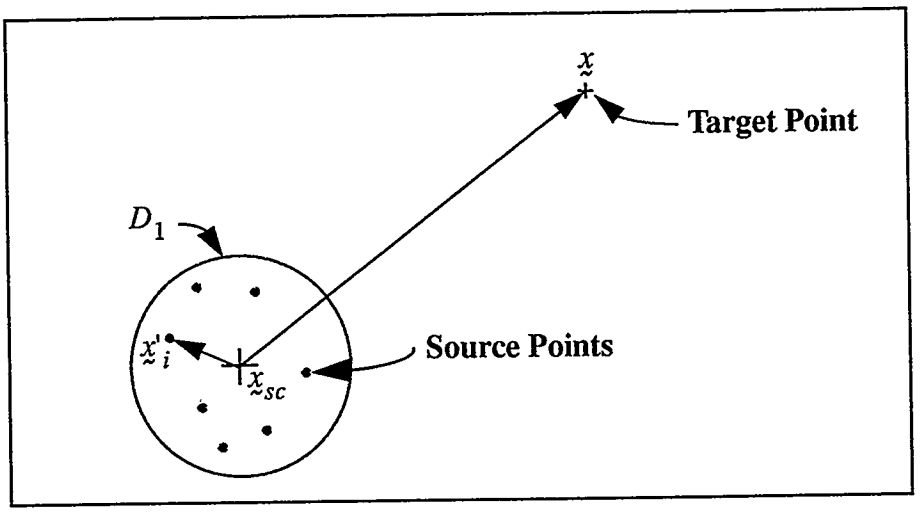

Figure 1. Multipole Expansion about Point in Source Domain

In order to illustrate the manner in which a multipole expansion may be generated, consider the simple one-dimensional example given by the equation:

$$\psi(x) = \sum_{i=1}^{N} W(x_i) K(x - x'_i) . \tag{8}$$

Our goal is to replace $K(x - x'_i)$ with a series expansion in which the variables x and x'_i are separated as in Equation 4. This may be easily achieved by expanding $K(x - x'_i)$ into a Taylor series about the point x_{sc} which is given by:

$$K(x - x'_i) = K(x - x_{sc}) - (x'_i - x_{sc}) K'(x - x_{sc}) + \frac{(x'_i - x_{sc})^2}{2!} K''(x - x_{sc}) - \dots . \tag{9}$$

We note that if x and x'_i are replaced by positions in the complex plane z and z'_i that we have a planar two-dimensional multipole expansion. The problem now reduces to finding the derivatives of K and making sure that the series converges to the desired accuracy in a reasonable number of terms.

For a specific example, consider the case in which $K(x) = \ln(|x|)$. From Equation 9:

$$K(|x - x'_i|) = \ln(|x - x_{sc}|) - \sum_{j=1}^{p-1} \left\{ \frac{1}{j} \left(\left| \frac{x'_j - x_{sc}}{x - x_{sc}} \right| \right)^j \right\} - O\left[\frac{1}{p} \left(\left| \frac{x'_j - x_{sc}}{x - x_{sc}} \right| \right)^p \right] . \tag{10}$$

We see that the resulting multipole series in x converges for $|x'_j - x_{sc}| < |x - x_{sc}|$ to an accuracy ε:

$$\varepsilon = O\left[\frac{1}{p} \left(\left| \frac{x'_j - x_{sc}}{x - x_{sc}} \right| \right)^p \right] . \tag{11}$$

As a second example, consider the axisymmetric vortex flow problem studied by Strickland and Amos [7]. The contribution to the stream-function at (x, r) from a group of N axisymmetric vortex rings located at (x'_i, r'_i) is given by:

$$\psi(x,r) = \sum_{i=1}^{N} W_i K(x, x'_i, r, r'_i) , \tag{12}$$

where

$$K(x, x'_i, r, r'_i) = r'_i r \int_0^{\infty} e^{-k|x-x'_i|} J_1(kr'_i) J_1(kr)\, dk . \tag{13}$$

A Taylor series expansion can be written for ψ as:

$$\psi = \sum_{n=0}^{p} \left\{ \sum_{m=0}^{n} \left[A_{n-m,m} \frac{\partial^n}{\partial x^{n-m} \partial r_{sc}^m} (K(x, x_{sc}, r, r_{sc})) \right] \right\} , \tag{14}$$

where

$$A_{n-m,m} = \sum_{i=1}^{N} \left[W_i \frac{(-x'_i + x_{sc})^{n-m} (r'_i - r_{sc})^m}{(n-m)!\, m!} \right] . \tag{15}$$

Here again we see that there is a separation of variables with regard to information concerning the source points (x'_i, r'_i) and the target point x, r. The most difficult step is to obtain the mixed partial derivatives of K as indicated in Equation 14. In this particular case, these derivatives were obtained as a function of associated Legendre functions of the second kind. It is of interest to note that the partial differential equation for the stream-function given by:

$$\frac{\partial^2 \psi}{\partial x^2} + \frac{\partial^2 \psi}{\partial r^2} = \frac{1}{r} \frac{\partial \psi}{\partial r} \tag{16}$$

can be used to develop two equations for K. This can be accomplished by noting that each vortex ring must individually satisfy Equation 16. Since for a single ring $\psi = WK$ with K equal to a constant then:

$$\frac{\partial^2 K}{\partial x^2} + \frac{\partial^2 K}{\partial r^2} = \frac{1}{r} \frac{\partial K}{\partial r} . \tag{17}$$

Also, due to the symmetry of the formulation the following is true:

$$\frac{\partial^2 K}{\partial x^2} + \frac{\partial^2 K}{\partial r_{sc}^2} = \frac{1}{r_{sc}} \frac{\partial K}{\partial r_{sc}} . \tag{18}$$

These relationships can be differentiated to obtain relationships between higher order partial derivatives. This in effect reduces the number of partial derivatives which have to be calculated directly from associated Legendre functions. Thus, we see that utilization of the governing partial equation may be very beneficial.

As a third example, consider the three-dimensional vector potential given by:

$$\underset{\sim}{\Psi}(r) = \sum_{i=1}^{N} \frac{\underset{\sim}{W}_i}{|r - r_i'|}. \tag{19}$$

Here r is the radial distance to the target point and r_i' is the radial distance to the source point. One could write Equation 19 in cartesian coordinates and obtain a Laurent series in x, y, and z for each component of $\underset{\sim}{\Psi}$. This has in fact been accomplished by Zhao [8]. Since Equation 19 is a solution to the Laplace equation, there are a number of relationships between the various partial derivatives associated with the Laurent series expansion which allows a reduction in the number of terms. An equivalent expansion which involves the use of spherical harmonics is given by Greengard [9] as:

$$\underset{\sim}{\Psi}(r) = \sum_{i=1}^{N} \sum_{n=0}^{p} \sum_{m=-n}^{n} \underset{\sim}{A}_n^m(r_i' - r_{sc}, \theta_i', \phi_i') \frac{Y_n^m(\theta, \phi)}{|r - r_{sc}|^{n+1}}. \tag{20}$$

Here, $Y_n^m(\theta, \phi)$ are spherical harmonics which are functions of the polar and azimuthal angles θ and ϕ associated with the target point. The radius to the center of expansion is given by r_{sc}. Since the coefficients $\underset{\sim}{A}_n^m$ are only a function of information available at the source points then we see that a separation of variables in the spirit of Equation 7 has been achieved.

As a last example, we will consider a case in which the derivatives associated with the Taylor series expansion can be conveniently represented by the use of a special function. The fast Gauss transform developed by Greengard and Strain [10] has a kernel given by:

$$K(x) = e^{-\alpha x^2}. \tag{21}$$

Direct application of Equation 9 to this problem (differentiation of $e^{-\alpha x^2}$) does not yield particularly satisfying results. However, if one notes that the derivatives of the kernel $K(x)$ can be written in terms of Hermite polynomials

$$K^n(x) \equiv \frac{d^n}{dx}\left(e^{-\alpha x^2}\right) = (-1)^n e^{-\alpha x^2} H_n(\sqrt{\alpha} x) \tag{22}$$

then the kernel can be easily expanded to obtain:

$$K(x - x_i') = e^{-(x - x_{sc})^2} \sum_{n=0}^{p} \frac{1}{n!} \left[\sqrt{\alpha}(x_i' - x_{sc})\right]^n H_n\left(\sqrt{\alpha}(x - x_{sc})\right). \tag{23}$$

Greengard and Strain [10] further extend this one-dimensional fast Gauss transform to multi-dimensions.

In summary, the far-field or multipole expansions allow one to separate variables such that $O(N)$ computations may be made. These expansions may be obtained by writing a Taylor series in a chosen coordinate system. The resulting series may be further simplified by making use of the governing differential equation along with perhaps a set of special functions.

2.2 Translation of Source Domain Center

An essential requirement for virtually all of the fast solution techniques it is to be able to shift the center of the multipole expansion $\underset{\sim}{x}_{sc}$ in domain D_1 to a new center located at $\underset{\sim}{x}'_{sc}$ in domain D_2 as indicated by Figure 2. This allows one to efficiently obtain multipole expansions in large domains by summing the contributions from shifted multipole expansions associated with a number of sub-domains.

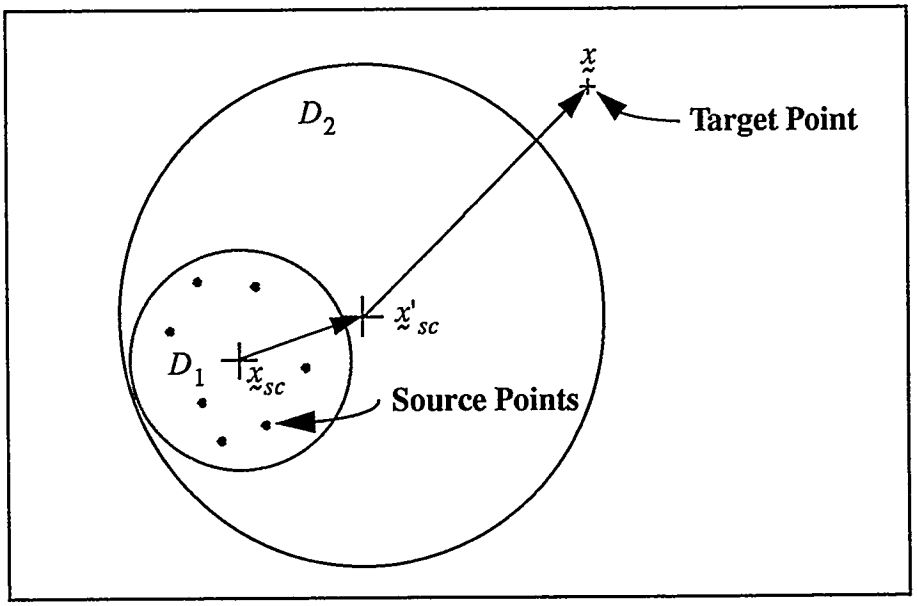

Figure 2. Translation of Source Domain Center

For the sake of brevity, we will not present shifted multipoles for all of the examples in the previous section but only consider the simplest case given by Equations 8 and 9 in order to illustrate the basic concept. From Equations 8 and 9 the function $\psi(x)$ may be written as:

$$\psi(x) = \sum_{n=0}^{p} \left[C_n(x'_i) \frac{d^n}{dx^n} K(x - x_{sc}) \right] + \varepsilon, \tag{24}$$

where

$$C_n(x'_i) = \sum_{i=1}^{N} \left[\frac{(-1)^n}{n!} W(x'_i) \, (x'_i - x_{sc})^n \right]. \tag{25}$$

In order to shift the expansion to the new center $\underset{\sim}{x}'_{sc}$ we rewrite Equation 24 as:

$$\psi(x) = \sum_{n=0}^{p} \left\{ C_n(x'_i) \frac{d^n}{dx^n} K\left[(x - x'_{sc}) - (x_{sc} - x'_{sc}) \right] \right\} + \varepsilon. \tag{26}$$

This can be written in terms of a new Taylor series given by:

$$\psi(x) = \sum_{n=0}^{p} \left[C'_n(x'_i) \frac{d^n}{dx^n} K(x - x'_{sc}) \right] + \varepsilon, \tag{27}$$

where

$$C'_n(x'_i) = \sum_{q=0}^{n} \left[\frac{(-1)^q}{q!} C_{n-q}(x'_i) \, (x_{sc} - x'_{sc})^q \right]. \qquad (28)$$

Thus if we have expansions for several groups of sources about several centers in domain D_2, then we can simply add their shifted coefficients $C'_n(x'_i)$ together to form a new far field expansion. The basic concept may be extended to multi-dimensional problems by using multi-dimensional Taylor series expansions. Various kernel functions may be used but they must always produce a convergent series and of course, one must be able to differentiate them if the series are formed using a Taylor series approach.

2.3 Local Expansion About Point in Target Domain

For many of the fast solution techniques, the far field or multipole expansion along with the ability to shift the expansion to a new center is all that is required. Greengard and Rokhlin [6] also take advantage of a local expansion about a point $\underset{\sim}{x}_{tc}$ in a target domain D_3 which is well separated from the source domain D_2. This local expansion allows one to obtain the influence of a group of sources on a target point as a function of the relative position between the target point at $\underset{\sim}{x}$ and the center of the local expansion at $\underset{\sim}{x}_{tc}$. This is sometimes referred to as a group-to-group interaction whereas the multipole expansion is a group-to-point interaction.

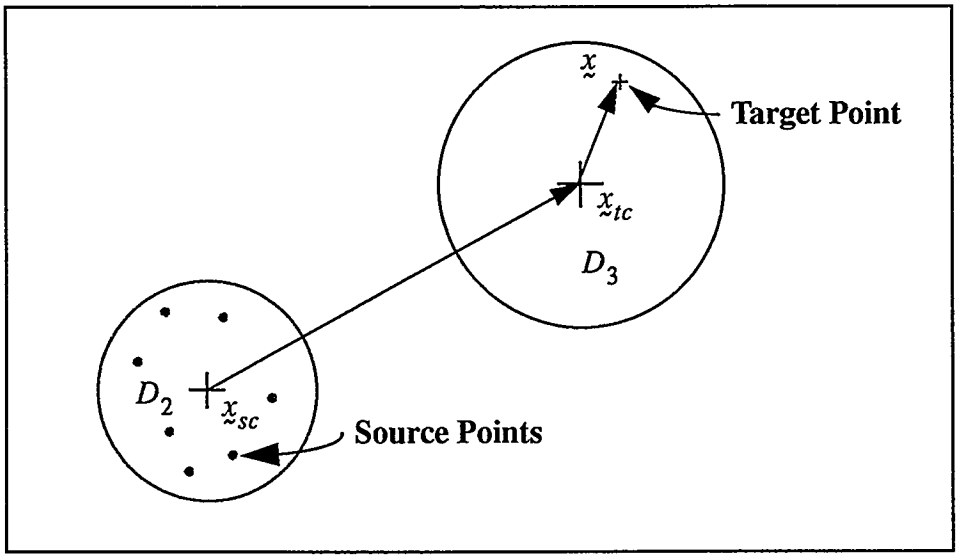

Figure 3. Local Expansion About Point in Target Domain

We can rewrite Equation 24 in the following form.

$$\psi(x) = \sum_{n=0}^{p} \left[C_n(x'_i) \frac{d^n}{dx^n} K\left[(x - x_{tc}) - (x_{sc} - x_{tc}) \right] \right] + \varepsilon \, . \qquad (29)$$

It should be noted that Equation 27 can also be written in this form if we simply let the shifted center of expansion for the multipole be relabeled as x_{sc}. Equation 29 can be expanded and

rewritten in terms of a local series given by:

$$\psi(x) = \sum_{n=0}^{p} \left[D_n(x'_i)\ (x - x_{tc})^n \right] + \varepsilon \tag{30}$$

where

$$D_n(x'_i) = \sum_{q=0}^{p-n} \left[\frac{C_q(x'_i)}{n!} \frac{\partial^{n+q}}{\partial x^{n+q}} K(x_{sc} - x_{tc}) \right]. \tag{31}$$

We note that Equation 30 is a power series in $(x - x_{tc})$. Typically, for higher dimensional problems a power series containing products of the independent variables will result.

2.4 Translation of Target Domain Center

Finally, for the Greengard Rokhlin method we must be able to shift the local expansion as indicated in Figure 4 from a center at $\underset{\sim}{x}_{tc}$ to a center at $\underset{\sim}{x}'_{tc}$.

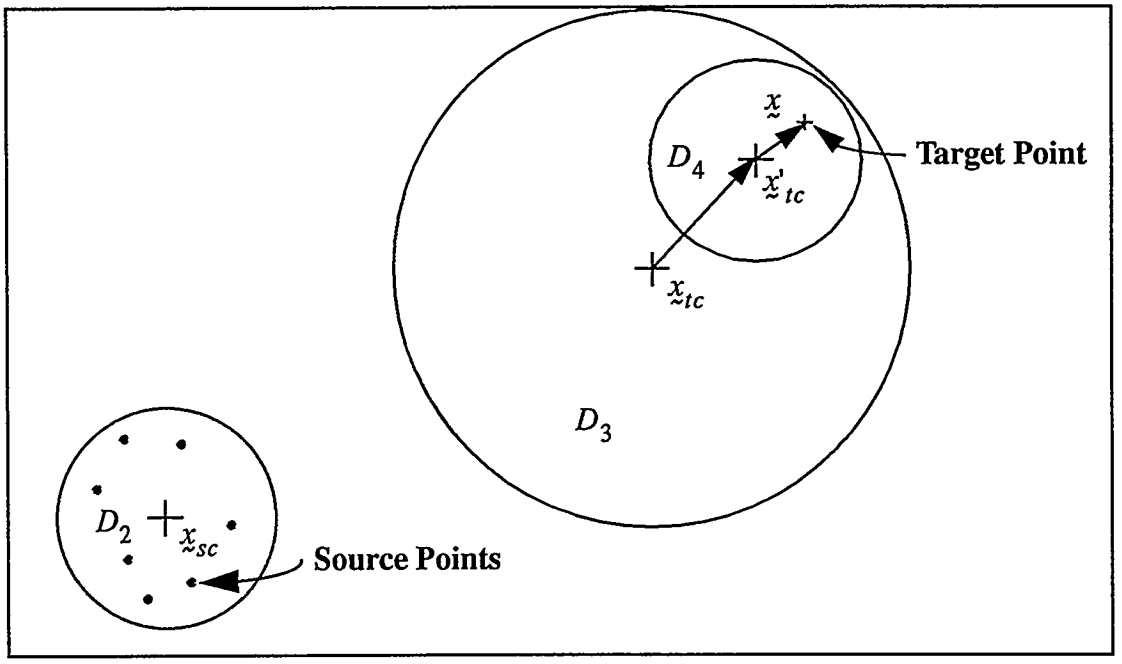

Figure 4. Translation of Target Domain Center

We first rewrite Equation 30 by inserting the center of the new target domain x'_{tc}.

$$\psi(x) = \sum_{n=0}^{p} \left[D_n(x'_i)\ [\,(x - x'_{tc}) - (x_{tc} - x'_{tc})\,]^n \right] + \varepsilon. \tag{32}$$

This can be rearranged to obtain a local power series in $x - x'_{tc}$ given by:

$$\psi(x) = \sum_{n=0}^{p} \left[D'_n(x'_i)\ (x - x'_{tc})^n \right] + \varepsilon, \tag{33}$$

where

$$D'_n(x'_i) = \sum_{q=0}^{p-n} \left[D_{n+q}(x'_i) \frac{(n+q)!}{n!q!} (x'_{tc} - x_{tc})^q \right]. \quad (34)$$

3 SPATIAL PARTITIONING

As discussed previously, the fast solution technique is predicated on the ability to separate variables into those containing information associated with the sources and those containing information associated with the target points. In order to accomplish this, the kernel is written in terms of truncated series expansions which are valid only under certain conditions. These conditions are generally associated with the separation between sources and target points. In order to insure that these conditions are met, one is required to develop some sort of scheme to quantify the relative separation between groups of sources and target points. Virtually all of the methods which have been developed thus far possess a tree structure or hierarchy produced by the division of the space containing source and target points into progressively smaller regions. In the following two sections we will present an overview of such schemes. The methods will be divided into two broad classes which we will loosely categorize as Barnes-Hut schemes and Greengard-Rokhlin schemes. The distinguishing difference between the two methods is that the Barnes-Hut scheme utilizes only far-field expansions while the Greengard-Rokhlin scheme utilizes both near-field and far-field expansions.

3.1 Barnes-Hut Schemes

Barnes and Hut [5] developed a fast algorithm to study the interaction of two spherical galaxies which are moving relative to each other and which are made up of several thousand particles. Their work was based in part on that of Appel [11] who also developed a fast algorithm to study the interaction of particles in a gravitational force field. Barnes and Hut improved the tree structure of Appel by regularizing the spatial partitioning and were thereby able to predict and improve the accuracy of the method. In both cases, the force on a target point was calculated using the gravitational force produced by the total mass of a source cluster assumed to be located at the cluster centroid. In essence, they used a far-field multipole expansion in which only the first two terms were retained. Translation of the source domain centers was achieved by calculating the centroid of the sources in the domain.

The tree-structure of Barnes and Hut was obtained by first surrounding the source and target points by a square (cube in three-dimensions) as indicated in Figure 5. This box is further subdivided into four squares (eight cubes in three-dimensions). Subdivision of parent boxes is continued until there is only one particle per box. Empty boxes are discarded. Each box is tagged with the total mass contained in the box and the center of gravity. This includes all of the parent boxes as well. The force on any particle is obtained by sequentially examining the boxes starting with the largest. The ratio of the source box size to the distance between the box center of gravity and the target point is checked to see if it is below a certain value or if there is only one particle in the box. This, of course, insures that a certain minimum accuracy will be maintained. If the error criteria is met, the contribution from that box is computed. If

not, the children of that box are examined to see if they in turn meet the error criteria. This process is carried out in such a manner so as to include the effect of every source in the field.

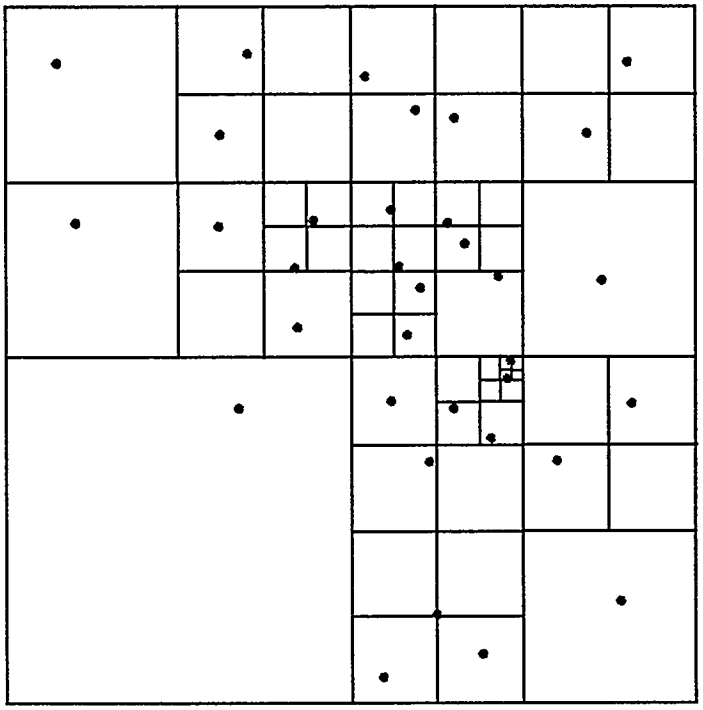

Figure 5. Barnes-Hut Hierarchical Boxing [5]

It should be pointed out, that the adaptive domain meshes which are generated here are not to be confused with the adaptive meshes which are generated for conventional CFD formulations. In the present case, the meshes represent a domain decomposition which is very simple when compared to meshes generated for conventional CFD formulations. Mesh generation for conventional CFD formulations is for the purpose of writing difference or element equations which satisfy the governing differential flow equations whereas the domain meshes generated here are for the purpose of grouping sources or target points. The domain meshes in the present case do not have to conform to any flow boundaries, they extend only to regions where sources or target points reside, and they are generated using a very simple algorithm. Generation of adaptive domain meshes is achieved using a very small amount of CPU time whereas adaptive mesh generation for conventional CFD problems can be quite CPU time intensive.

The Barnes-Hut algorithm, in its original form, is very simple. The multipole algorithm which they used and the associated translation operation were simple but only of first order. The hierarchical box structure had to have a large number of levels in order to insure that each particle would eventually be isolated. One obvious improvement to the original Barnes-Hut algorithm is to use higher order multipoles which improves the accuracy and decreases the number of levels in the box hierarchy. For example, McMillan and Aarseth [12] applied the Barnes-Hut algorithm to a stellar dynamics problem in which they used up to 8 terms in the multipole expansion.

Van Dommelen and Rundensteiner [13] developed an algorithm in which they used high order multipoles with 13 to 23 terms to model vortex interactions. They found that in order to optimize the procedure, each childless box should contain about 100 particles (vortices). They also used a binary box numbering scheme which had the position and size of the box encrypted into it.

Clarke and Tutty [14] found that with the number of multipole terms equal to 25, approximately 30 vortices in a box was optimum. However, the spatial decomposition used by Clarke and Tutty was different than that used in the original Barnes-Hut algorithm. As shown in Figure 6, the original box is divided into only two smaller boxes with half of the particles in each box. The boxes are rectangular and extend only far enough to capture half of the particles. At each step, the rectangular parent boxes are subdivided along their major axis in order to form relatively square child boxes. This method is very efficient in that the number of particles in each box at each level is essentially constant. This also allows one to start out with a rectangular box of any aspect ratio instead of a square one.

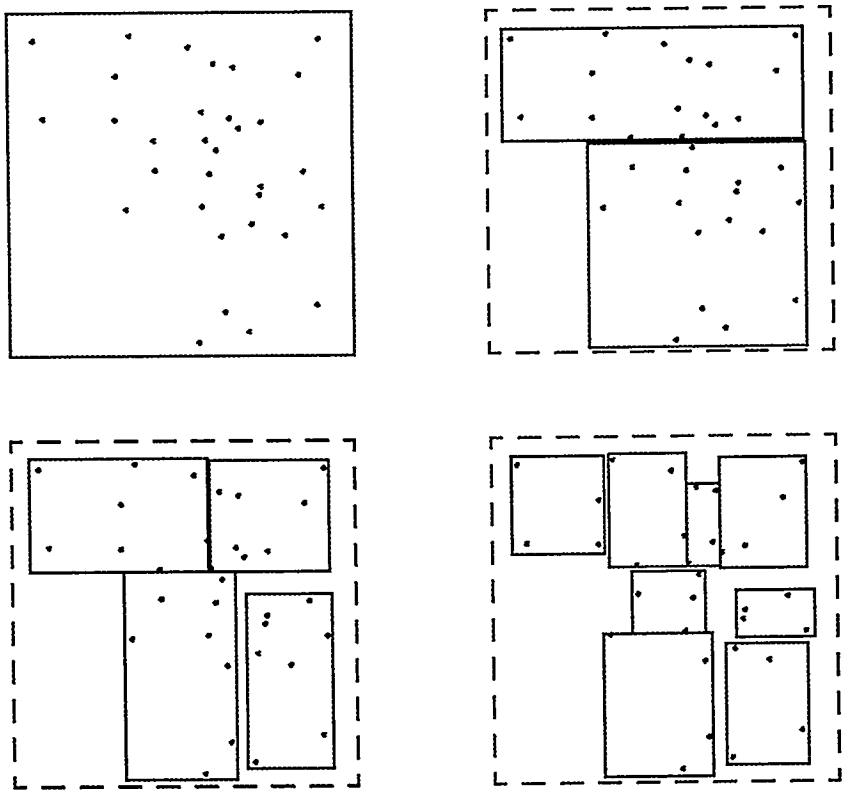

Figure 6. Clarke and Tutty Spatial Decomposition [14]

Another variation of the binary tree spatial decomposition is presented in the work of Draghicescu [15], [16]. In this method, the original box may be square or rectangular with an aspect ratio equal to two. As each box is divided into two halves, a pair of rectangles with aspect ratio equal to two or a pair of squares will result. While this approach is not as adaptive as the Clarke and Tutty method with regard to maintaining a uniform number of particles

in each box at a given level, it is somewhat less complex. It is certainly more adaptive than the quad or oct trees associated with the original Barnes-Hut method.

We close this section by noting that there are a large number of possible variations with regard to spatial decomposition. For example, in an interesting paper by Niedermeier and Tavan [17] on the dynamics of proteins produced by electrostatic interactions, the spatial decomposition is based on the structural features of the proteins themselves. The structural features of a certain protein allows them to develop an electrostatic model for individual protein molecules which may then be used in a dynamic analysis of a system of molecules.

3.2 Greengard-Rokhlin Schemes

As mentioned previously, the distinguishing difference between the two methods which have come to be known as the Barnes-Hut and Greengard-Rokhlin schemes is that in addition to utilizing far-field expansions the Greengard-Rokhlin scheme also takes advantage of near-field or local expansions. This idea is clearly presented in a paper by Rokhlin [18] which predates the work by Barnes and Hut and no doubt formed the basis for the ensuing work by Greengard and Rokhlin [6], [19] as well as that of Carrier, Greengard, and Rokhlin [20]. The Greengard and Rokhlin method allows one to compute the influence of a cluster of source points on a cluster of target points in a very efficient manner. The Barnes-Hut method, on the other hand, allows one to compute the influence of a cluster of sources on a single target point in an efficient manner.

In the original Greengard-Rokhlin schemes [6], [19], the domain decomposition is non-adaptive, meaning that the domain is broken up into a set of uniform squares or cubes. The two-dimensional adaptive domain decomposition used in the work of Carrier, Greengard, and Rokhlin [20] is identical to that shown in Figure 5 except that there are typically more than one source point per box. For the adaptive scheme, a somewhat involved procedure is used to define the separation condition between a particular target box and each of the source boxes. This procedure determines the way in which sources in a particular source box influence the target points in a particular target box. In general, each target box at each level has five possible relationships with each source box in the mesh. A formal description of these "box lists" will not be given here, but in general, the five lists produce the following types of restrictions on the use of the series expansions:

1. Direct calculations must be made. Multipole and local series expansions cannot be used.
2. Both multipole and local series expansions can be used.
3. Multipole series expansions can be used, local series expansions cannot.
4. Local series expansions can be used, multipole expansions cannot.
5. Contributions from distant source boxes reside in the parent of the target box.

These lists are illustrated in Figures 7 and 8 for the cross-hatched target boxes. It is assumed that there are sources in all boxes. In Figure 7a, the list 1, 2, 3, and 4 source boxes are shown for the 2x2 target box. Figures 7b, 8a, and 8b illustrate how information from other parts of the domain is brought in through ancestors of the target box in Figure 7a.

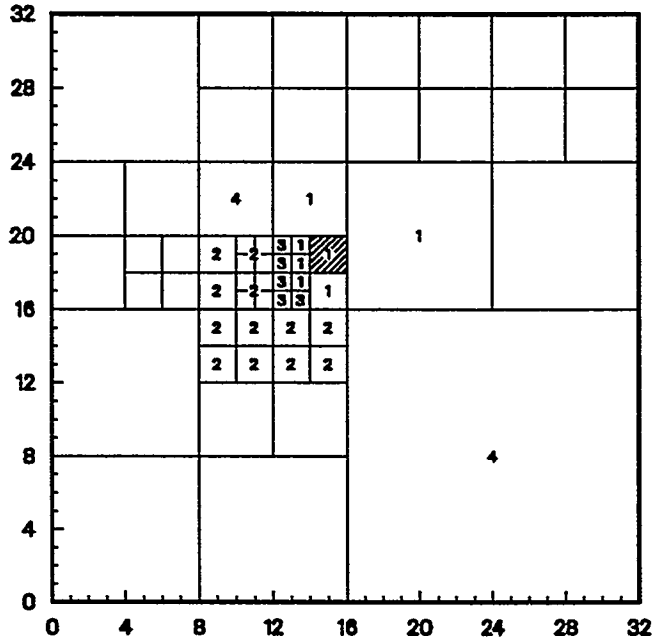

a) Contribution from childless target box's own box list.

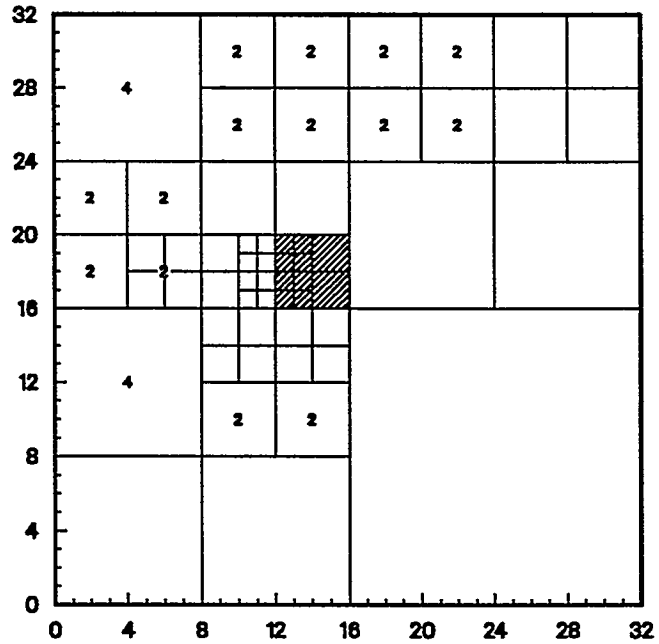

b) Contribution from childless target box's parent's box list.

Figure 7. Box List Example

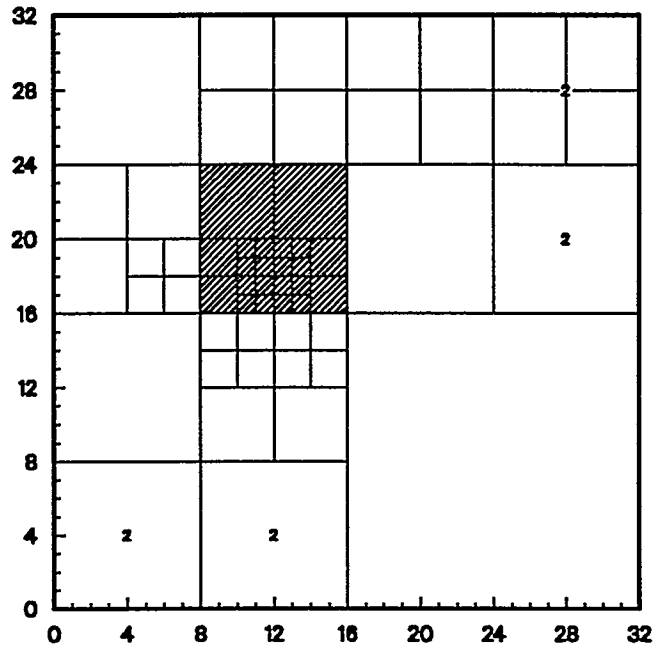

c) Contribution from childless target box's grandparent's box list.

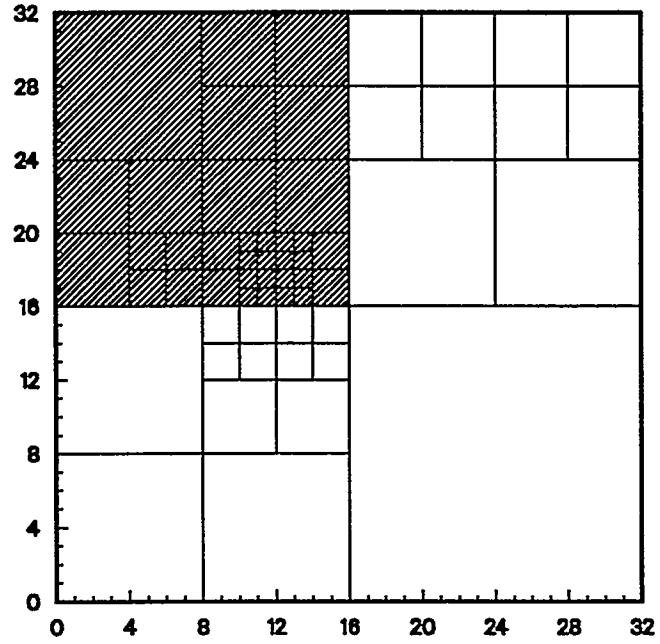

d) Contribution from childless target box's great grandparent's box list.

Figure 8. Box List Example (continued)

The Greengard-Rokhlin algorithm is significantly more complex than the Barnes-Hut algorithm especially when applied in an adaptive manner. It is perhaps for this reason that there have not been very many extensions to the basic concept. Schmidt and Lee [21] developed an algorithm for including periodic boundary conditions for the purpose of evaluating Coulomb potentials in a three-dimensional non-adaptive scheme. Strickland and Amos [7] used the adaptive technique of Carrier, Greengard, and Rokhlin [20] with a new kernel to solve for the stream function associated with axisymmetric vortical flow fields. Strickland and Baty [22] have written an adaptive three-dimensional code for the vector potential. In order to allow the source and target points to be different sets, hierarchical meshes for both the source and target points are constructed by this algorithm. The authors report that this code is under further development to include the FFT fast shift algorithms of Greengard and Rokhlin [23]. Aluru [24] has conceptualized a method which should make this and other hierarchical schemes more efficient by effectively removing redundant nodes in the tree which contain information about the same set of particles.

3.3 Comparison of Methods

In this section we provide a brief comparison of the methods. As noted previously, the Greengard-Rokhlin algorithm is significantly more complex than the Barnes-Hut algorithm and is more memory intensive. The apparent advantage of the Greengard-Rokhlin algorithm is its execution time of $O(N)$ whereas the Barnes-Hut method executes in $O(N\ln N)$.

There is some dispute in the literature about the $O(N)$ dependance for the Greengard-Rokhlin algorithm. For instance, Aluru [24] has hypothesized that both methods will execute in $O(N\ln N)$ but only after redundant nodes in the hierarchical tree structures are removed. His argument is based in part on the fact that creation of the tree structure requires $O(N\ln N)$ work. However, experience has shown that the amount of time required to create the tree structure for the Greengard-Rokhlin algorithm is trivial compared to the rest of the calculation. The major portion of the calculation, on the other hand, tends to scale like $O(N)$ depending on the distribution of the particles. Simulations in which the particle distributions tend to be non-uniform (especially concentrated along lines or surfaces) generally execute in $O(N)$ time. While creation of the tree may indeed require $O(N\ln N)$ operations, the constant of proportionality apparently is relatively small.

Blelloch and Narlikar [25] made a direct comparison for the potential problem between the three-dimensional Barnes-Hut and Greengard-Rokhlin methods. They found that at a high level of accuracy (RMS-error $< 10^{-5}$), the Greengard-Rokhlin method was faster than the Barnes-Hut method for $N > 10^4$, assuming a random distribution of points. At a lower level of accuracy (RMS-error $< 10^{-3}$), the Greengard-Rokhlin method did not outperform Barnes-Hut until $N > 10^8$. Both algorithms were implemented on parallel machines. Thus, we see that the choice of methodology is a function of the number of particles in the field and the error requirements.

We also note that memory requirements may also play a role. The Greengard-Rokhlin method requires more memory than the Barnes-Hut algorithm since both the far-field and local expansions for each box at each level must be retained.

4 PARALLELIZATION

This section discusses briefly two approaches which have been developed to parallelize the numerical evaluation of the discrete N-body problem given by Equation 2. The parallelization of the N-body problem is currently a very active area of computational research; therefore, a general discussion is beyond the scope of the present paper.

Over the last several years, a significant amount of research has been directed toward developing and implementing algorithms to evaluate efficiently the discrete N-body problem on parallel computers. While some of this work has focused on general parallelization methods, a great deal of it has emphasized specific computer architectures and codes. Two techniques applied commonly are hierarchical methods and direct methods. Most parallelizations of the N-body problem utilize one or both of these methods. In a general sense, the hierarchical methods include both the tree method of Barnes and Hut [5] and the fast multipole method of Greengard and Rokhlin [6] discussed in this paper.

Greengard and Gropp [26] have developed a parallel two-dimensional non-adaptive fast multipole method for the Encore Multimax 320 computer. In this work, Greengard and Gropp parallelized the computation of the initial moments and the evaluation of the local series expansions and found that the main limitation was the coordination of the processors required in passing information between the different mesh levels. For the details of the performance of this scheme see [26]. Work on a parallel version of an adaptive fast multipole method has presented in Singh et al. [27], while Zhao and Johnsson [28] have developed a parallel three-dimensional multipole method for the Connection CM-2 computer. Work on a parallel version of the tree method of Barnes and Hut has also been presented, for example see Salmon [29] and Grama et al. [30].

Parallel versions of the direct method have also been developed. This approach makes no attempt to simplify or reduce Equation 2 before it is parallelized. An example of this approach is given in the recent technical note of Stiller et al. [31]. In this work, some simple coding procedures are given which have been shown to speed up the direct method an order of magnitude on the massively parallel computer CM-200. A further example of a parallelized direct method and its application to vortex methods is given by Sethian et al. [32].

5 EXAMPLE CALCULATIONS

In the following examples, we present a mixture of model problems and physical simulations. In the model problems, the distributions of source and target points are prescribed. These problems allow one to carefully benchmark the performance of the various methods in terms of CPU time, accuracy, and the specified geometry. Most of the physical simulations represent an evolutionary process in which the sources and targets may be moving at each time step.

5.1 A Two-Dimensional Fast Adaptive Multipole Code

Carrier, Greengard, and Rokhlin [20] developed a two-dimensional adaptive code which is an extension of the two-dimensional non-adaptive code of Greengard and Rokhlin [6]. This code

was used to obtain the potential and electrostatic field due to a distribution of charged particles. The precision was set so as to yield an RMS error roughly equal to single precision on a VAX-8600 which they were using (10^{-5} to 10^{-6}).

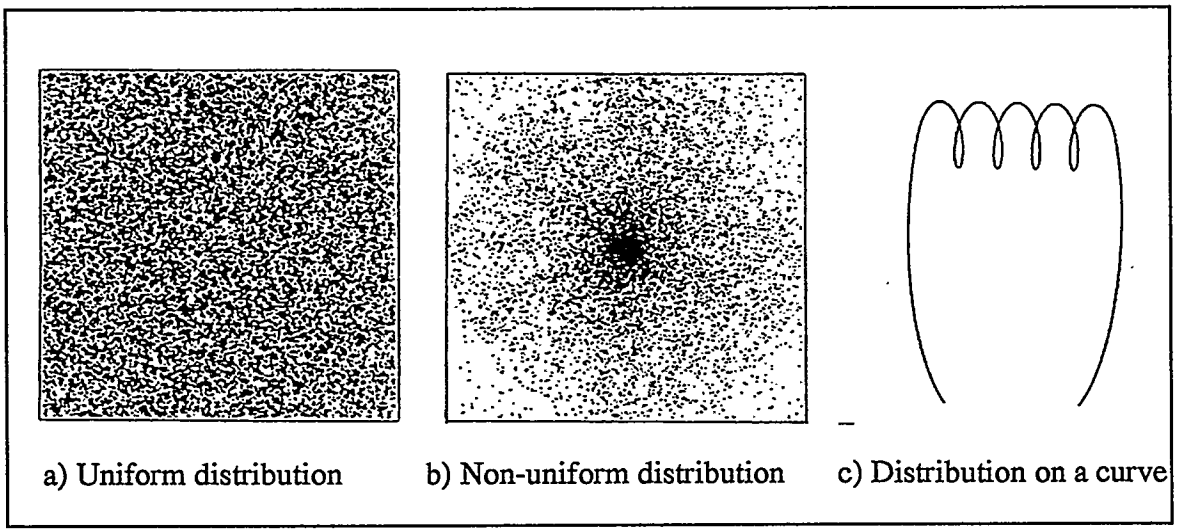

Figure 9. Benchmark Distributions

Three benchmark source and target distributions which they studied are indicated in Figure 9. For a benchmark problem in which 25,600 sources and targets were uniformly distributed in a square, the direct solution required 9694 seconds while the non-adaptive algorithm required 138 seconds, and the adaptive algorithm required 97 seconds. For a highly non-uniform distribution in a square, the direct and adaptive methods performed essentially as before while the non-adaptive algorithm required 2318 CPU seconds. For all of the points distributed along a curve, the direct solution performed as before, the non-adaptive algorithm required 152 seconds, while the adaptive algorithm required only 48 seconds. It should be noted that the adaptive algorithm performed as an $O(N)$ algorithm for this case but not for the other two distributions.

5.2 A Three-Dimensional Fast Adaptive Multipole Code

Strickland and Baty [22] developed an extended version of the three-dimensional Greengard algorithm [9]. This algorithm is adaptive and features a box hierarchy for the sources which may be different from that of the targets. In this code, each component of the vector potential is first obtained. For the case where the vector potential is used to represent a blob of vorticity, the curl of the vector potential yields the velocity vector. Thus we see that this code is required to do more than three times as much work as one which calculates a simple scalar potential. Three different sets of source and target point distributions used to benchmark the method are shown in Figure 10. In each case, the number of sources and targets were both equal to N.

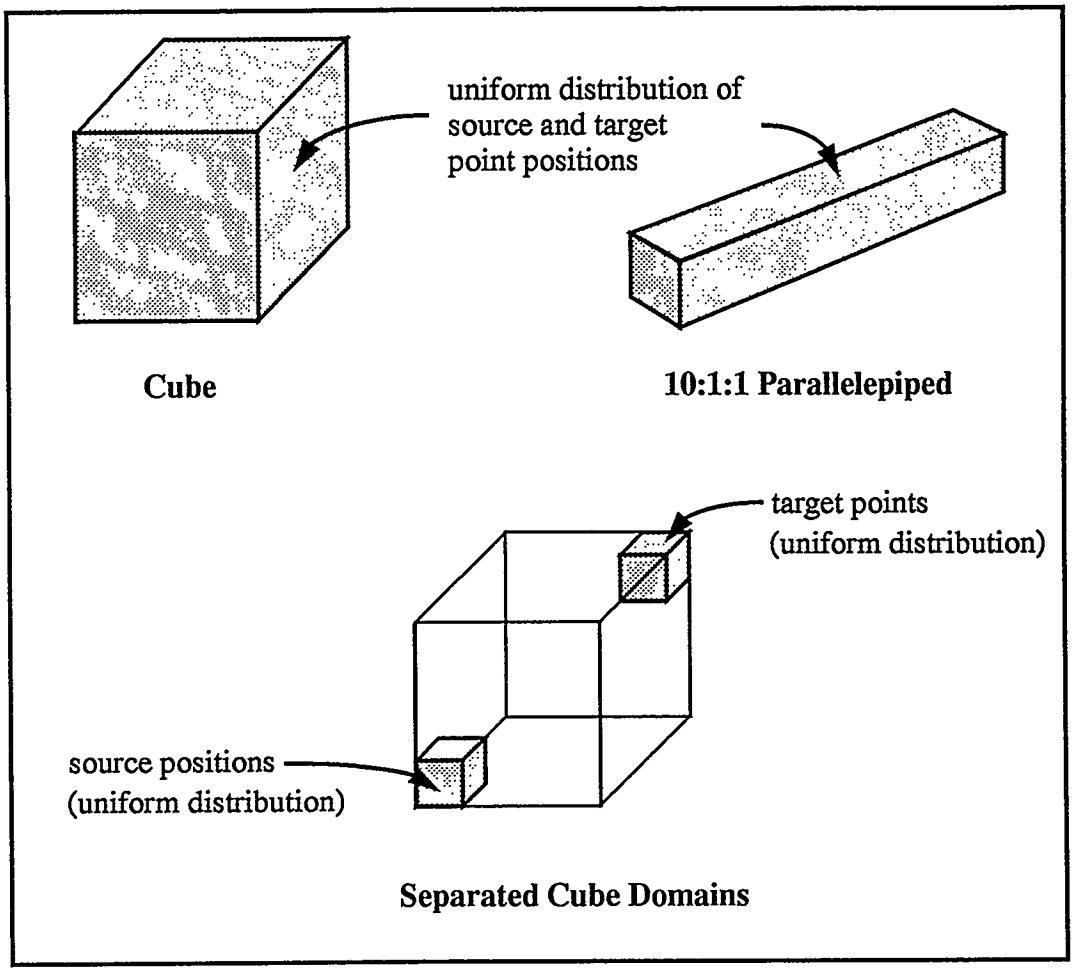

Figure 10. Benchmark Configurations

The code was run at a precision such that the RMS error in the magnitude of the velocity vector would be on the order of 0.1%. The RMS error in the magnitude of the vector potential was one to two orders of magnitude less than that associated with the velocity vector. All runs were made on a SUN Sparc 10 workstation. For the cube domain the fast solver was faster than direct calculations for $N > 5000$ and was an order of magnitude faster for $N = 100,000$. Computation time for the fast solver was about 8,000 seconds. For the parallelepiped configuration, the break-even point occurred slightly earlier at $N = 3000$ but the CPU times for $N = 100,000$ were essentially the same as for the cube configuration. For the separated cube domain configuration, the break-even occurred at $N = 1000$ with the fast solver requiring only 800 seconds of CPU time for $N = 100,000$. In this later case, the fast solution technique truly performed as an $O(N)$ algorithm,

5.3 Fast Gauss Transform

Greengard and Strain [10] used their fast Gauss transform (case number 3 in table 1) to make calculations for N sources at N target points for the two geometries shown in Figure 11. The source and target point locations are congruent. In Figure 11a the points are distributed uni-

formly in a unit square while in Figure 11b the points are distributed uniformly on a unit circle. Computations using several different levels of precision and numbers of source and target points were made. For $N = 102,400$ the direct solution required more than 8 days of CPU time on a Sun-4 workstation. Using the fast method, the solution for the square was obtained in only 9 minutes and the solution for the circle was obtained in only 5 minutes. Errors normalized by the total source strengths were approximately 5×10^{-10} and 4×10^{-11} for the square and circle respectively.

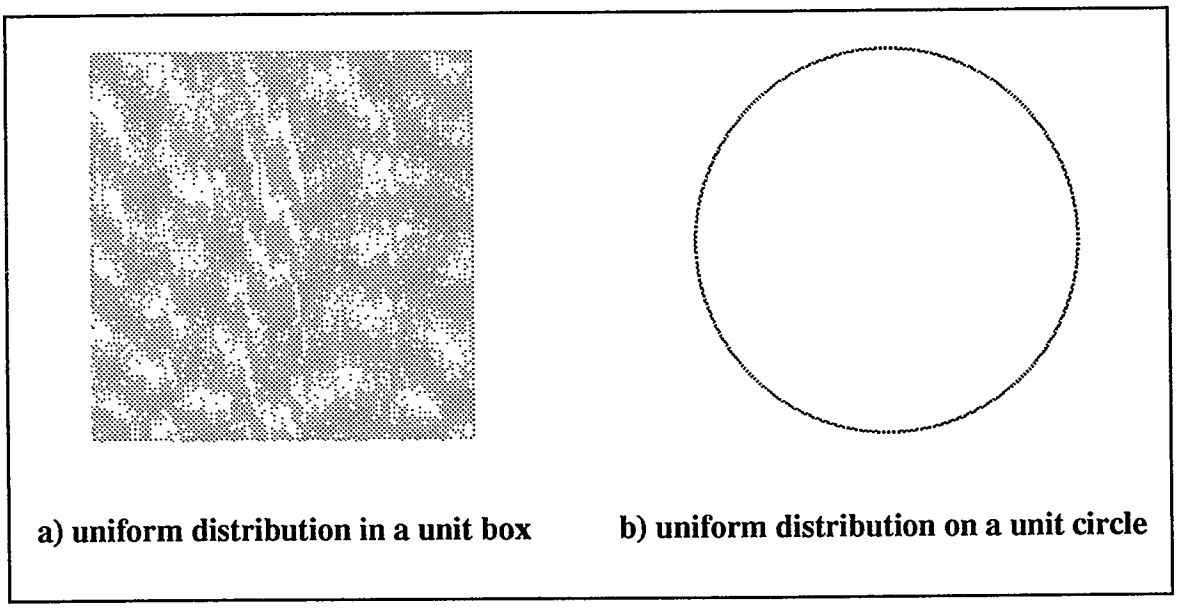

a) uniform distribution in a unit box **b) uniform distribution on a unit circle**

Figure 11. Example Fast Gauss Transform Source and Target Distributions

5.4 An Axisymmetric Bluff-Body Flow

The stream function and velocity components produced by axisymmetric ring vortices are much more expensive to compute than for those produced by vortices associated with the two-dimensional planar case. As mentioned previously, Strickland and Amos [7] developed a fast multipole algorithm based upon the adaptive Carrier, Greengard, and Rokhlin method [20] but utilizing the kernel associated with the stream function for axisymmetric ring vortices. This algorithm breaks even for $N = 100$ and is about 30 to 100 times faster than the direct solver for $N = 10,000$. Precisions for the velocity calculations were set to produce RMS errors on the order of 0.1%. Errors associated with the stream function were one to two orders of magnitude lower. The original benchmark studies were run on a VAX-8600. The CPU time required to compute the field for $N = 10,000$ ranged from about 400 seconds to about 1350 seconds. Present runs on a SUN Sparc 10 are roughly an order of magnitude faster.

Strickland [33] developed an axisymmetric vortex code to study the flow over parachutes and other axisymmetric shells which utilizes this fast solver. In the work of Higuchi, Balligand, and Strickland [34] unsteady flow over a disk was simulated and compared with experimental

results. The disk was first accelerated to a constant velocity, held at that velocity for about three diameters of travel, and then decelerated to rest. In Figure 12, experimental flow visualization of the wake is shown just after the disk begins to decelerate and just prior to its coming to rest. Also, the experimental drag coefficient C_d versus non-dimensional tome T is shown along with simulation data obtained from the fast vortex method (FVM).

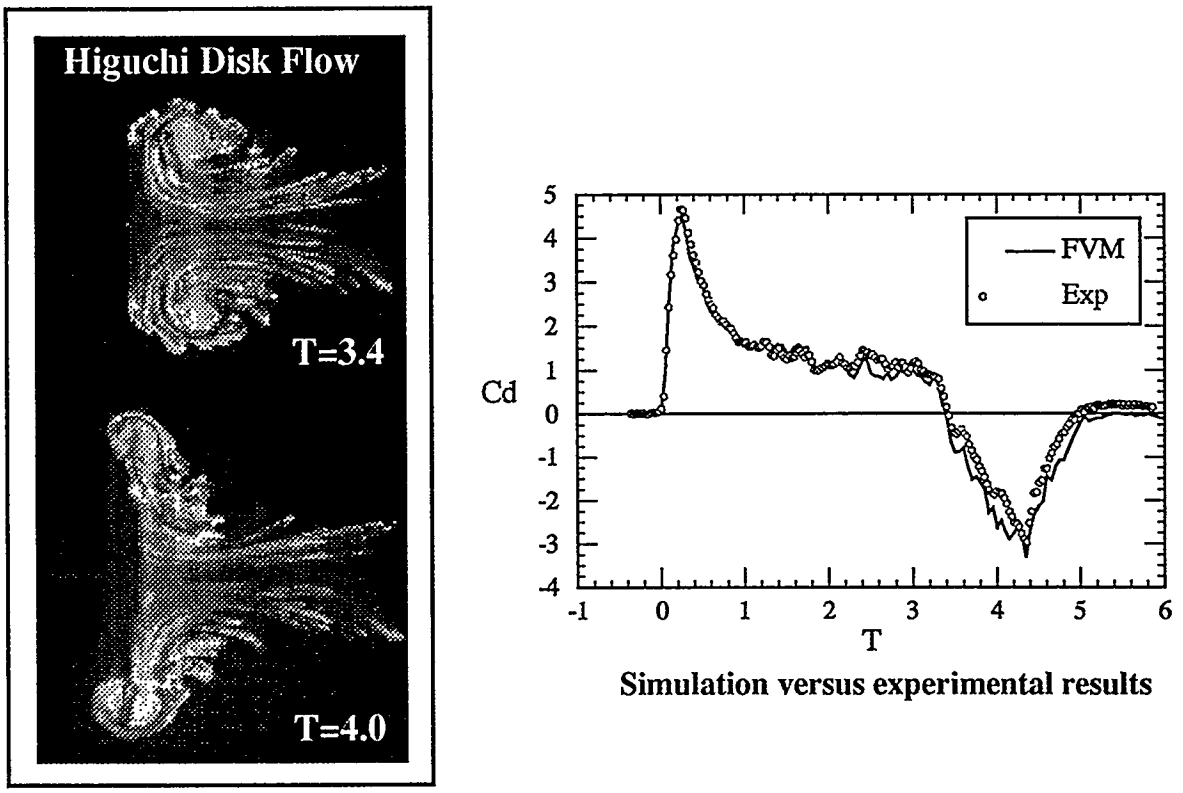

Figure 12. Simulation of Unsteady Flow over a Disk

5.5 An Astrophysics Simulation

Salmon, Warren, and Winckelmans [35] present a gravitational simulation of the formation of large scale structures in the universe. The particles in their simulation "represent the so-called "Dark Matter" which is believed to dominate the mass of the universe." The region which they simulated was "a sphere containing 1,099,135 bodies." Each of these bodies had a mass of 3.3×10^7 solar masses. A snapshot of the simulation is shown in Figure 13 at a late period in the evolution after significant clumping has occurred.

They used a Touchstone Delta system to perform the computations. The original Barnes-Hut scheme was used in which the three-dimensional space was divided into an adaptive oct-tree and the mass and center of mass provided a two-term multipole. They describe in some detail the methodology which they used in parallelizing the code. For 512 processors, approximately 50 seconds was required to compute a single time step with 1×10^6 bodies. With 32 processors the time increased to approximately 400 seconds per time step.

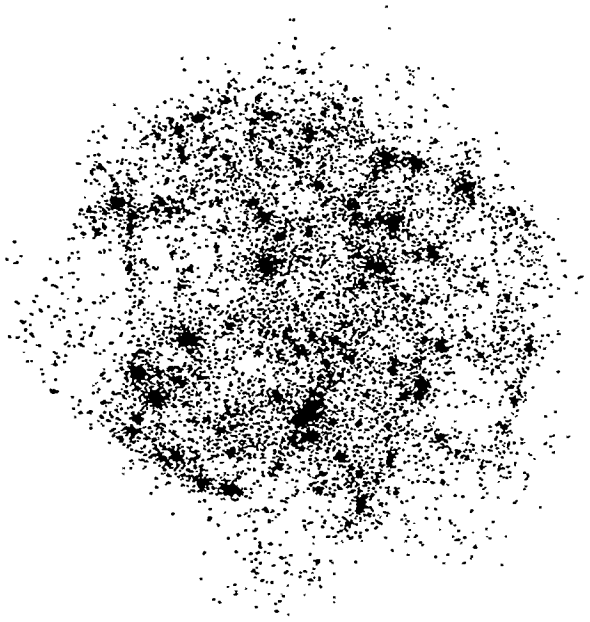

Figure 13. Clumping of Dark Matter in the Universe

5.6 Flow Past a Pitching Airfoil

The Barnes-Hut method of Van Dommelen and Rundensteiner [13] was used to reduce the CPU time for a vortex simulation produced by Shih, Lourenco, Van Dommelen, and Krothapalli [36] of flow over a pitching airfoil. In Figure 14, the vorticity which has been generated at the airfoil surface is shown as discrete points along with the instantaneous streamlines. In Figure 15 the calculated streamlines are compared with experimentally obtained iso-vorticity lines. We note that the streamlines and iso-vorticity lines display the same flow morphology.

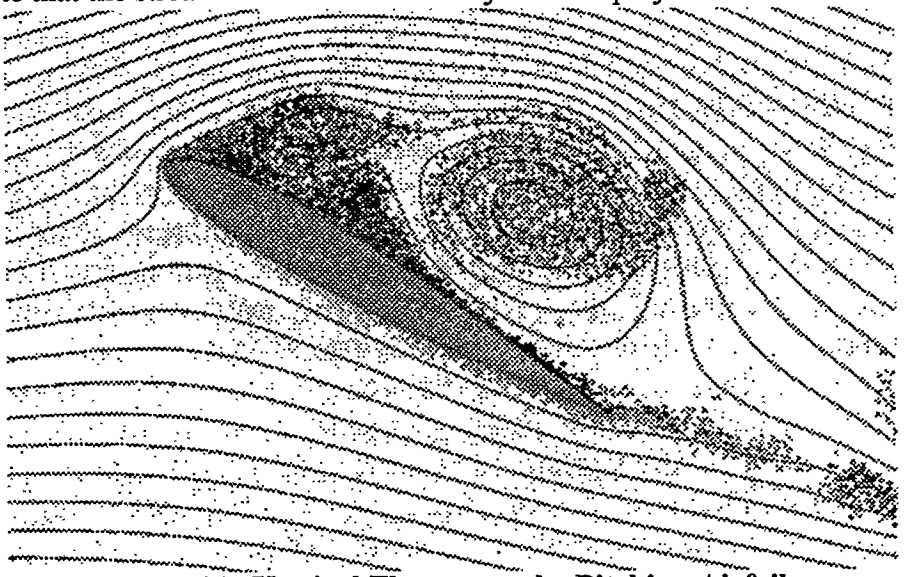

Figure 14. Vortical Flow around a Pitching Airfoil

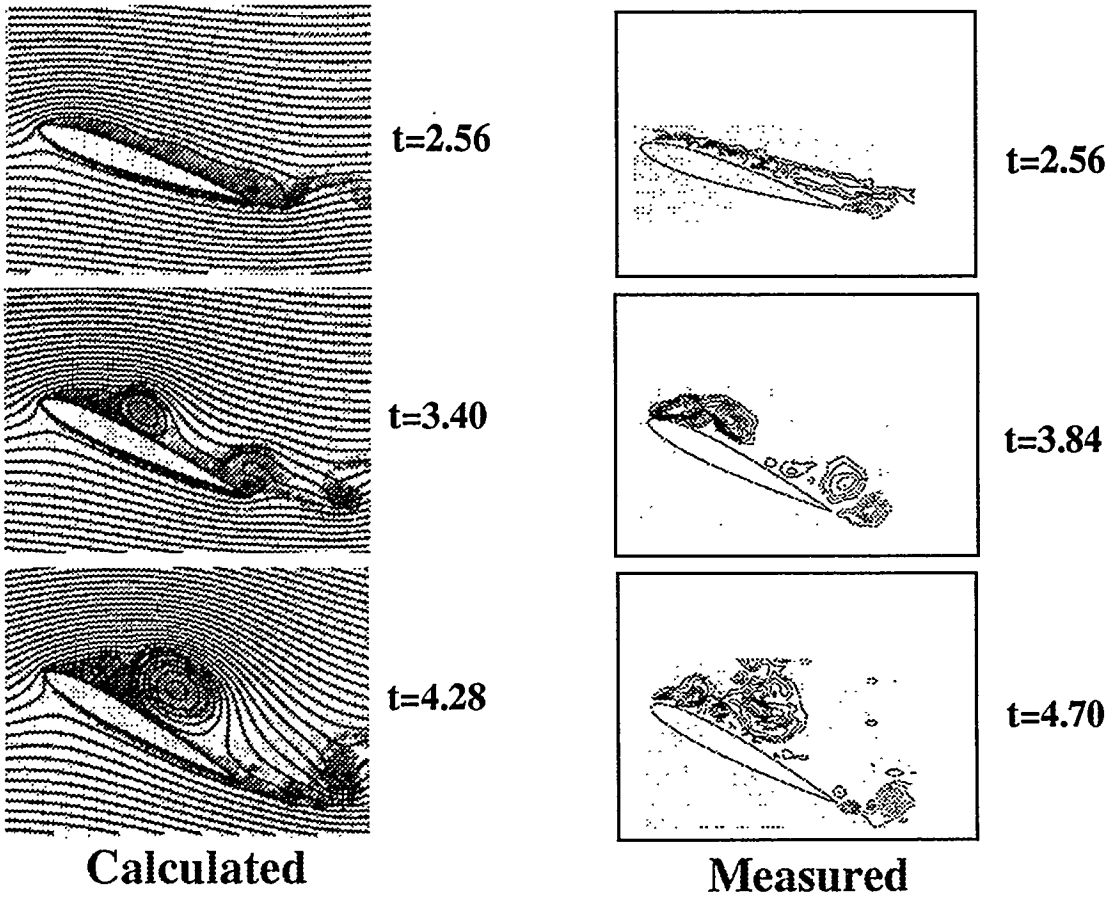

Figure 15. Calculated Streamlines and Measured Iso-Vorticity Lines

Reportedly, this simulation required up to 32,000 vortices at the later time steps. The CPU time for these later steps would have been on the order of several minutes per time step when running on a CYBER 205 had the fast solver not been used. According to [13], the computation using the fast solver should be between 13 and 28 times faster.

6 CONCLUSIONS

We have presented an overview of several fast multipole methods and several simulations which rely upon their use. We believe that these fast algorithms and their extensions represent a very important numerical tool for the following reasons:

1. There are a very large number of physical and numerical problems which may be cast in terms of Equations 2 and 4.
2. Many of these problems are intractable without the efficiencies afforded by these fast methods.
3. In the future, the solution of much larger "N-body" problems will be required in order to advance numerical simulation capabilities. The difference between an $O(N^2)$, $O(N\ln N)$, and $O(N)$ simulation will become even more important.

7 REFERENCES

[1] Roach, G. F., *Green's Functions*, second edition, Cambridge University Press, p. 141, 1982.

[2] Greengard, L., "Fast Algorithms for Classical Physics," *Science*, Vol. 265, pp. 909-914, August 1994.

[3] Batchelor, G. K., *An Introduction to Fluid Dynamics*, Cambridge University Press, pp. 84-87, 1992.

[4] Hassani, S., *Foundations of Mathematical Physics*, Allyn & Bacon, pp. 841-846, 1991.

[5] Barnes, J. E. and Hut, P., "A Hierarchical $O(N\log N)$ Force Calculation Algorithm," *Nature*, Vol. 324, No. 4, pp. 446-449, December 1986.

[6] Greengard, L. and Rokhlin, V. "A Fast Algorithm for Particle Simulations," *J. Compt. Phys.*, Vol. 73, pp. 325-348, 1987.

[7] Strickland, J. H., Amos, D. E., "A Fast Solver for Systems of Axisymmetric Ring Vortices," Sandia National Laboratory Report SAND90-1925, 52 pages, September (1990). Also *AIAA Journal*, Vol. 30, No. 3, pp. 737-746, March 1992.

[8] Zhao, F., An $O(N)$ Algorithm for Three-Dimensional N-Body Simulations, M. S. Thesis, Massachusetts Institute of Technology, Boston MA, 1987.

[9] Greengard, L., "The Rapid Evaluation of Potential Fields in Particle Systems," Yale University Report YALEU/DCS/RR-533, April 1987.

[10] Greengard, L. and Strain, J., "The Fast Gauss Transform," *SIAM J. Sci. Stat. Comput.*, Vol. 12, No. 1, pp79-94, January 1991.

[11] Appel, A. W., "An efficient Program for Many-Body Simulation," *SIAM J. Sci. Stat. Comput.*, Vol. 6, No. 1, pp. 85-103, January 1985.

[12] McMillan, S. L. W. and Aarseth, S. J., "An $O(N\ln N)$ Integration Scheme for Collisional Stellar Systems," *The Astrophysics Journal*, Vol. 414, pp. 200-212, September 1993.

[13] Van Dommelen, L. and Rundensteiner, E., "Fast, Adaptive Summation of Point Forces in the Two-Dimensional Poisson Equation," *J. Compt. Phys.*, Vol. 83, pp. 126-147, 1989.

[14] Clarke, N. R. and Tutty, O. R., "Construction and Validation of a Discrete Vortex Method For The Two-Dimensional Incompressible Navier-Stokes Equations," *Computers Fluids*, Vol. 23, No. 6, pp. 751-783, 1994.

[15] Draghicescu, C. I., "An Efficient Implementation of Particle Methods For The Incompressible Euler Equations," *SIAM J. Numer. Anal.*, Vol. 31, No. 4, pp. 10909-1108, August 1994.

[16] Draghicescu, C. I and Draghicescu, M., "A Fast Algorithm for Vortex Blob Interactions," *J. Compt. Phys.*, Vol. 116, pp. 69-78, 1995.

[17] Niedermeier, C. and Tavan, P., "A Structure Adapted Multipole Method for Electrostatic Interactions in Protein Dynamics," *J. Chem. Phys.*, Vol. 101, No. 1, pp. 734-740, July 1994.

[18] Rokhlin, V., "Rapid Solution of Integral Equations of Classical Potential Theory," *J. Compt. Phys.*, Vol. 60, pp. 187-207, 1983.

[19] Greengard, L. and Rokhlin, V., "On the Efficient Implementation of the Fast Multipole Algorithm," Yale University Report YALEU/DCS/RR-602, February 1988.

[20] Carrier, J., Greengard, L., and Rokhlin, V., "A Fast Adaptive Multipole Algorithm for Particle Simulations," *SIAM Journal on Scientific and Statistical Computing*, Vol.9, No.4, pp.669-696, July 1988.

[21] Schmidt, K. E. and Lee, M. A., "Implementing the Fast Multipole Method in Three Dimensions," *J. Stat. Phy.*, Vol. 63, Nos. 5/6, 1991.

[22] Strickland, J. H., and Baty, R. S., "A Three-Dimensional Fast Solver for Arbitrary Vorton Distributions," Sandia National Laboratories Report SAND93-1641, May 1994.

[23] Greengard, L. and Rokhlin, V., "On the Efficient Implementation of the Fast Multipole Algorithm," Yale University Report YALEU/DCS/RR-602, February 1988.

[24] Aluru, S., "Distribution-Independent Hierarchical N-body Methods," Ph.D. Dissertation, Iowa State University, Ames, Iowa, 1994.

[25] Belloch, G. and Narlikar, G., "A Comparison of two N-Body Algorithms," School of Computer Science, Carnegie Mellon University, October 1994.

[26] Greengard, L. and Gropp, W. D., "A Parallel Version of The Fast Multipole Method," *Computers Math. Applic.*, Vol. 20, No. 7, pp. 63-71, 1990.

[27] Singh, J. P., Holt, C., Hennessy, J. L., and Gupta, A., "A Parallel Adaptive Fast Multipole Method," IEEE Conference SUPERCOMPUTER'93.

[28] Zhao, F., Johnsson, S. L., "The Parallel Multipole Method on the Connection Machine," *SIAM J. Sci. & Stat. Compt.*, Vol. 12, No. 6, 1991.

[29] Salmon J., "Parallel $N\log N$ N-Body Algorithms and Applications to Astrophysics," IEEE Conference COMPCON Spring 91.

[30] Grama, A. Y., Kumar, V., and Sameh, A., "Scalable Parallel Formulations for the Barnes-Hut Method for N-Body Simulations," Proceedings of Supercomputing'94.

[31] Stiller, L., Daemen, L. L., and Gubernatis, J. E., "N-Body Simulations on Massively Parallel Architectures," *J. Compt. Phys.*, Vol. 115, 1994.

[32] Sethian, J. A., Brunet, J. P., Greenberg, A., and Mesirov, J. P., "Vortex Methods and Massively Parallel Processors," *Lectures in Applied Mathematics*, Vol. 28, 1991.

[33] Strickland, J. H., "A Prediction Method For Unsteady Axisymmetric Flow Over Parachutes," *AIAA Journal of Aircraft*, Vol. 31, No. 3, pp. 637-643, May-June 1994.

[34] Higuchi, H., Balligand, H., and Strickland, J. H., "Numerical and Experimental Investigations of the Unsteady Flow Over a Disk," Forum on Vortex Methods for Engineering Applications, Sandia National Laboratories, Albuquerque NM, pp. 277-297, February 22-24, 1995.

[35] Salmon, J. K., Warren, M. S., and Winkelmans, G. S., "Fast Parallel Tree Codes for Gravitational and Fluid Dynamical N-Body Problems," *Int. J. Supercomputer App. & High Perf. Comp.*, Vol. 8, No. 2, pp. 129-142, Summer 1994.

[36] Shih, C., Lourenco, Van Dommelen, L., and Krothapalli, "Unsteady Flow Past an Airfoil Pitching at a Constant Rate," *AIAA Journal*, Vol. 30, No. 5, pp. 1153-1161, May 1992.

(this page intentionally left blank)

Distribution

Dr. Harlow G. Ahlstrom
Boeing Defense & Space Group
P.O. Box 3999, MS85-85
Seattle WA 98124-2499

Prof. Christopher Anderson
4068 Blackbird Way
Callabassi CA 91302

Analytical Methods (2)
P.O. Box 3786
Bellevue, WA 98009
Attn: F. Dvorak
B. Maskew

Prof Hassan Aref
Dept. of Applied Mech. and Eng. Sci.
University of California
La Jolla, CA 92093

Prof. Andrew S. Arena Jr..
School of Mech. and Aero. Eng.
Oklahoma State University
Stillwater, OK 74078-0545

Prof. Holt Ashley
Dept. of Aero. and Astronautics
Stanford University
Stanford, CA 94305

Prof. Bruce Bayly
Mathematics Department
University of Arizona
Tucson, AZ 85721

Dr. P. W. Bearman
Dept. of Aeronautics
Imperial College
London, SW7 2BY
ENGLAND

Prof. James Brasseur
Dept. Mech Eng.
The Pennsylvania State University
University Park, PA 16802

Dr. J. Carrier
124 Me Pierre Termier
73000 Chambery, FRANCE

Prof. A. J. Chorin
Department of Mathematics
University of California
Berkeley, CA 94720

Dr. David J. Cockrell
Department of Engineering
University of Leicester
Leicester, LE1 7RH
ENGLAND

Prof. Werner Dahm
Dept. Aerospace Engineering
University of Michigan
Ann Arbor, MI 48109-2118

Dr. M. R. Dhanak
Dept. Ocean Engineering
Florida Atlantic University
Boca Raton, FL 33431

Dr. Karl F. Doherr
Head, Applied Math. Branch
DLR, Institut fur Flugmedanile
Flughafen, D33
Braunschweig
GERMANY

Dr. Feri Farassat
NASA Langley Rearch Center
Mail Stop 460
Hampton, VA 23681-0001

Prof. Ahmed F. Ghoniem
Dept. of Mech. Eng.
Mass. Inst. of Tech.
Cambridge, MA 02139
Prof. Peyman Givi
Dept. of Mech. and Aero Eng.
State University of New York
Buffalo, NY 14260-4400

Dr. John R. Grant
Naval Undersea Center
1176 Howell Street
Building 108, Code 8233
Newport RI 02841-1708

Prof. Leslie Greengard
Courant Institute of Math. Sciences
New York University
251 Mercer Street
New York, NY 10012

Prof. G. Gregorek
Dept. of Aero. and Astronautics
Ohio State University
2070 Neil Avenue
Columbus, OH 43210

Capt. Hank Helin
HQ USFA/DFAN
USAF Academy, CO 80840-5701

Prof. H. Higuchi
Dept. of Mech. & Aero. Eng.
Syracuse University
Syracuse, NY 13244

Prof. A. K. M. F Hussain
Dept. of Mech. Eng.
University of Houston
Houston, TX 77204-4792

Prof. Yassin A. Jassan
Nuclear Engineering Dept.
Texas A&M University
College Station, TX 77843

Prof. Joseph Katz
Dept. Aerospace Eng. and Eng. Mech.
San Diego State University
San Diego, CA 92182-0183
Prof.Mitsuru Kurosaka
Dept. of Aeronautics and Astronautics
Mail Stop FS-10
University of Washington
Seattle, WA 98195

Prof. Anthony Leonard
Graduate Aeronautics Lab.
California Institute of Technology
Pasadena, CA 91125

Dr. William W. Liou
ICOMP
NASA Lewis Research Center
Cleveland, OH 44135

Prof. Mark D. Maughmer
Department of Aerospace Engineering
The Pennsylvania State University
University Park, PA 16802

Dr. Jeffery S. Marshall
Iowa Institute of Hydraulic Research
University of Iowa
300 S. Riverside Drive
Iowa City, IA 52242-1585

Dr. Eckart Meiburg
Dept. of Aerospace Eng.
University of Southern California
854 W. 36th Place
Los Angeles, CA 90089-1191

Dr. D. I. Meiron
Dept. of Applied Mathematics
California Institute of Technology
Pasadena, CA 91125

Prof. R. N. Meroney
Dept. of Civil Eng.
Colorado State University
Fort Collins, CO 80521

Prof. Philip J. Morris
Department of Aerospace Engineering
The Pennsylvania State University
University Park, PA 16802
NASA Johnson Space Center (2)
Attn: EG3
Houston, Tx 77058
Attn: D. B. Kanipe
R. E. Meyerson

New Mexico State University (2)
Dept. of Mech. Eng.
Las Cruces, NM 88003
Attn: Ron Pederson
G. Reynolds

Dr. Monika Nitsche
Program in Applied Mathematics
Campus Box 562
University of Colorado
Boulder, Colorado 80309-0526

Prof. Ronald L. Panton
Dept. of Mech. Eng.
University of Texas
Austin, TX 78712

Prof. Ion Paraschivoiu
Dept. of Mech. Eng.
Ecole Polytecnique
CP 6079
Succursale A
Montreal H3C 3A7
CANADA

Prof. V. Rokhlin
Department of Computer Science
Yale University
PO Box 2158
New Haven, CT 06520

Prof. Ralph Rosenbaum
School of Physics
Tel Aviv University
Ramat - Aviv, 69978
ISRAEL

Prof. P. G. Saffman
Dept. of Applied Mathematics
California Institute of Technology
Pasadena, CA 91125

Prof. William Saric
Dept of Mech. and Aerospace Eng.
Arizona State University
PO Box 876106
Tempe, AZ 85287-6106

Prof. T. Sarpkaya
Dept. Mech. Eng.
Code 69-SL
Naval Postgraduate Academy
Monterey, CA 93943

Dr. Klaus Schilling
FH Ravensburg-Weingarten
Postfach 1261
D-7987 Weingarten
GERMANY

Dr. John M. Seiner
NASA Langley Research Center
Mail Stop 165
Hampton, VA 23681-0001

Prof. J. A. Sethian
Dept. of Mathematics
University of California
Berkely, CA 94720

Dr. Karim Shariff
NASA-Ames Research Center
MS: 202A-1
Moffet Field, CA 94035-1000

Dr. David Sharpe
Department of Aeronautical Eng.
Queen Mary College
Mile End Road
London, E1 4NS
ENGLAND

Prof. Roger L. Simpson
Dept. Aerospace and Ocean Eng.
Virginia Polytechnic Institute
and State University
Blacksburg, VA 24061

Prof. John A. Strain
Department of Mathematics
University of California
Berkeley, CA 94720

Texas Tech University (2)
Dept. of Mech. Eng.
Lubbock, TX 79409
Attn: J. H. Lawrence
J. W. Oler
Dr. Boyko Tchavdarov
KaTRI
Kajima Corporation
2-19-1,Tobitakyu,Chofu-Shi
Tokyo 182, Japan

Prof. G. Trygvasson
Dept. Mech. Eng. and App. Mech.
University of Michigan
Ann Arbor, MI 48109-2125

Prof. Don H. Tucker
Department of Mathematics
University of Utah
Salt Lake City, UT 84112

University of New Mexico (2)
Dept. of Mech. Eng.
Albuquerque, NM 87106
Attn: M. S. Ingber
C. R. Truman

Dr. James Uhlman
Code 804, Bldg. 108/2
Naval Undersea Warfare Center
Newport, RI 02841-5047

U. S. Army, Natick (9)
RD&E Center
AMED/ETD
Kansas St.
Natick, MA 01760
Attn: John Caligeros
Maurice Gionfriddo
Steven Kunz
Calvin Lee
Andrew Mawn
Robert Rodier
James Sadeck
Earl Steeves
Gary Thibault

Prof. Bruce R. White
Dept. of Mech. Eng.
2052 Bainer Hall
University of California
Davis, CA 95616

Prof. C. W. Van Atta
Dept. of App. Mech. and Eng. Sci.
Mail Code 0411
University of California
La Jolla CA 92093-0411

Prof. L. Van Dommelen
Dept. of Mech. Eng.
Florida State University
PO Box 2175
Tallahassee, FL 32316-2175

Washington State University (3)
Dept. Mech. & Matl's Eng.
Pullman, WA 99164-2920
Attn: Jacob Chung
Clayton Crowe
Tim Troutt

Prof. R. E. Wilson
Dept. Mech. Eng.
Oregon State University
Corvallis, OR 97331

Dr. G. S. Winklemans
Mech. Eng. Dept.
University of Sherbrooke
Sherbrooke, Quebec
JIK-2R1
CANADA

Prof. Norman J. Zabusky
Dept. of Mech. and Aerospace Eng.
Rutgers University
PO Box 909
Piscataway, NJ 08855-0909

Dr. David Zielke
Naval Research Lab, 6-4-40
4555 Overlook Avenue, SW
Washington, DC 20375

MS0310	2416	J. M. Macha
MS0149	4000	J. C. Cummings
MS0811	4918	S. P. Goudy
MS0574	5941	D. F. Wolf
MS0704	6201	P. C. Klimas
MS0708	6214	H. M. Dodd
MS0708	6214	D. E. Berg
MS9051	8351	L. A. Rahn
MS9051	8351	W. T. Ashurst
MS9053	8366	C. M. Hartwig
MS9401	8700	R. C. Wayne
MS9043	8743	M. L. Callabresi
MS9043	8745	R. J. Kee
MS0841	9100	P. J. Hommert
MS0828	9102	R. D. Skocypec
MS0833	9103	J. H. Biffle
MS0828	9104	E. D. Gorham

MS0827	9111	W. L. Hermina
MS0827	9111	C. E. Hickox
MS0827	9111	S. N. Kempka
MS0827	9111	J. A.Schutt
MS0834	9112	A. C. Ratzel
MS0835	9113	S. E. Gianoulakis
MS0835	9113	R. J. Cochran
MS0827	9114	R. T. McGrath
MS0827	9114	C. C. Wong
MS0825	9115	W. H. Rutledge
MS0825	9115	D. P. Aeschliman
MS0825	9115	R. S. Baty (5)
MS0825	9115	F. G. Blottner
MS0825	9115	J. K. Cole
MS0825	9115	W. L. Oberkampf
MS0836	9116	C. W. Peterson
MS0836	9116	V. L. Behr
MS0836	9116	L. A. Gritzo
MS0836	9116	G. F. Homicz
MS0836	9116	D. D. McBride
MS0836	9116	J. M. Nelsen
MS0836	9116	J. H. Strickland (15)
MS0836	9116	D. W. Sundberg
MS0836	9116	S. R. Tieszen
MS0836	9116	D. E. Waye
MS0836	9116	W. P. Wolfe
MS0443	9117	H. S. Morgan
MS0443	9117	A. E. Hodapp
MS0437	9118	E. P. Chen
MS0437	9118	F. J. Mello
MS0437	9118	J. W. Swegle
MS0321	9200	E. H. Barsis
MS1111	9221	S. S. Dosanjh
MS1111	9221	D. W. Barnette
MS1110	9222	R. C. Allen
MS1110	9222	L. Romero
MS0819	9231	A. C. Robinson
MS0819	9231	T. G. Trucano
MS0439	9234	D. R. Martinez
MS0951	9621	R. A. LaFarge
MS9018	8523-2	Central Technical Files
MS0899	4414	Technical Library (5)
MS0619	12615	Print Media
MS0100	7613-2	Document Processing For DOE/OSTI (2)

Org.	Bldg.	Name	Rec'd by	Org.	Bldg.	Name	Rec'd by

Sandia National Laboratories